

RESEARCH ARTICLE

WILEY

Investigation of the surfactant distribution in oil-in-water emulsions during the crystallization of the dispersed phase via nuclear magnetic resonance relaxometry and diffusometry

Gina Kaysan¹  | Raphael Kräling¹ | Manuel Meier² | Hermann Nirschl² | Gisela Guthausen^{2,3}  | Matthias Kind¹ 

¹Institute for Thermal Process Engineering, Karlsruhe Institute of Technology, Karlsruhe, Germany

²Institute for Mechanical Engineering and Mechanics, Karlsruhe Institute of Technology, Karlsruhe, Germany

³Engler-Bunte Institut, Water Chemistry and Water Technology, Karlsruhe Institute of Technology, Karlsruhe, Germany

Correspondence

Matthias Kind, Institute for Thermal Process Engineering, KIT, Karlsruhe 76131, Germany.

Email: matthias.kind@kit.edu

Abstract

The crystallization of melt emulsions is of great interest to the food, cosmetic, and pharmaceutical industries. Surfactants are used in emulsions and suspensions to stabilize the dispersed phase; thus, questions arise about the liquid–liquid and solid–liquid interfaces of the droplets or particles and the distribution of the surfactant in the different phases (continuous and dispersed phase, interface). Nuclear magnetic resonance relaxation and diffusion measurements revealed that the internal and rotational mobility of surfactant molecules at the liquid–liquid interface decreases with increasing droplet sizes. Additionally, solid–liquid interfaces have fewer surfactants than liquid–liquid interfaces as a result of the desorption of the surfactant molecules during the crystallization of the droplets. Relaxation rates of surfactant molecules in aqueous solution as single molecules, micelles, and at the liquid–liquid and solid–liquid interface are analyzed for the first time.

KEYWORDS

¹H, binary mixture, crystallization, desorption, diffusion, emulsion, interface, interfacial loading, micelles, NMR, relaxation, surfactant, surfactant distribution, Tween[®]20

1 | INTRODUCTION

Oil-in-water (O/W) emulsions with (partly) crystalline dispersed phases are increasingly applied in the fields of nutrition, health care, pharmaceutical, and automotive industry (coatings and lubricants).^[1] They are thermodynamically unstable colloidal systems, with one phase being dispersed in the other, the so-called continuous phase. Surface-active agents (surfactants) are used for

stabilization. Surfactants lower the surface tension of the droplets and reduce effects that cause emulsion break-ages, such as coalescence and Ostwald ripening.

Surfactants have an amphiphilic character due to a lipophilic or nonpolar part and a hydrophilic or polar part. Surfactant molecules form micelles (agglomerates of surfactant molecules) above the critical micelle concentration (*cmc*) in the aqueous continuous phase, in addition to their presence as single molecules, and adsorb to

This is an open access article under the terms of the [Creative Commons Attribution-NonCommercial-NoDerivs](https://creativecommons.org/licenses/by-nc-nd/4.0/) License, which permits use and distribution in any medium, provided the original work is properly cited, the use is non-commercial and no modifications or adaptations are made.

© 2022 The Authors. *Magnetic Resonance in Chemistry* published by John Wiley & Sons Ltd.

the liquid–liquid interface of the droplets up to the equilibrium surface loading. For example, we refer to Köhler and Schuchmann^[2] for an overview.

The critical packing parameter R_c can be used to describe the structure of micelles.^[3] R_c for Tween[®]20 (TW20), micelles is calculated as 0.09 (according to Tanford^[4] and Carnero Ruiz [5]), leading to the assumption of spherical micelles.

Details of a surfactant's distribution during crystallization of the dispersed phase are of high interest and importance.^[5] In addition to stabilizing two-phase systems by assembling at liquid–liquid interfaces, surfactants can also assemble at liquid–solid interfaces, such as in suspensions (e.g., Guardia et al.^[6]). Although for many aspects quite important, it is yet unknown how the surfactant is distributed in emulsions with (semi-) crystalline dispersed phases.

Finding out more about the distribution of surfactants in melt emulsions is of great importance, for example, to explain the contact-mediated nucleation.^[7–9] Adsorbed surfactants may shield the droplets from close contact with each other and hinder contact-mediated nucleation. In addition, knowledge about the surfactant distribution in the emulsion is important to describe the short- and long-term stability of emulsions and suspensions.

The influence of the surfactant on crystallization was studied especially in the field of solid–liquid nanoparticles.^[10] The focus is on the influence of surfactants on the morphology or melting temperature.

In a previous work, we showed that the surfactant concentration in the organic dispersed phase at equilibrium is low and neglectable compared to the concentration in the continuous phase.^[8] Here, we aim to obtain information about the distribution of the surfactants at the liquid–liquid and the solid–liquid interfaces during the crystallization of the dispersed phase. Such information reveals influencing factors of contact-mediated nucleation, as two blank interfaces of a molten and a crystallized droplet must be in contact for successful inoculation. Thus, an n-hexadecane-D₂O emulsion stabilized by the surfactant TW20 is investigated by nuclear magnetic resonance (NMR) spectroscopic, diffusion, and relaxation measurements.

2 | MODELING OF SIGNAL DECAYS OF NMR RELAXATION AND DIFFUSION MEASUREMENTS

The decay of signal intensity $S(q)$ of TW20 obtained from NMR diffusion measurements can be modeled using the gamma distribution according to Röding et al.^[11]:

$$S(q) = S_0 \left(1 + q^2 \left(\Delta - \frac{\delta}{3} \right) \frac{\sigma_{\text{eff,diff}}^2}{\langle D_{\text{eff}} \rangle} \right)^{-\frac{\langle D_{\text{eff}}^2 \rangle}{\sigma_{\text{eff,diff}}^2}} \quad (1)$$

Δ represents the diffusion time and S_0 the NMR amplitude at a gradient $g = 0 \text{ T m}^{-1}$. The parameter q is a function of the gyromagnetic ratio γ and the effective gradient duration δ :

$$q = \gamma \delta g. \quad (2)$$

This approach results in a mean, effective diffusion coefficient $\langle D_{\text{eff}} \rangle$, and effective distribution width of diffusion coefficients $\sigma_{\text{eff,diff}}$ of the gamma distribution.

The different species of TW20 (single molecules, in micelles, at liquid–liquid or solid–liquid surface) in an emulsion contribute in their specific way to the signal decay dominantly as a function of g . The effective diffusion coefficient is the sum of the effective diffusion coefficients of the different species i $\langle D_{\text{eff},i} \rangle$, weighted by the corresponding fractions x_i in a first approximation. The following assumptions are made for Equations (3) and (4): A monomodal distribution is assumed for each component due to an effective, averaged diffusion coefficient on the experimental time scale, and an exchange of the different moieties is considered. In this approach, $\langle D_{\text{eff},i} \rangle$ represents the effective diffusion coefficient of the following surfactant species: single molecules ($i = \text{sm}$), micelles ($i = \text{mic}$), and molecules at the interface ($i = \text{if}$). We assume the following relations:

$$\langle D_{\text{eff}} \rangle = x_{\text{sm}} \cdot \langle D_{\text{eff,sm}} \rangle + x_{\text{mic}} \cdot \langle D_{\text{eff,mic}} \rangle + x_{\text{if}} \cdot \langle D_{\text{eff,if}} \rangle, \quad (3)$$

$$\sigma_{\text{eff,diff}} = x_{\text{sm}} \cdot \sigma_{\text{eff,diff,sm}} + x_{\text{mic}} \cdot \sigma_{\text{eff,diff,mic}} + x_{\text{if}} \cdot \sigma_{\text{eff,diff,if}} \quad (4)$$

with

$$x_{\text{sm}} + x_{\text{mic}} + x_{\text{if}} = 1. \quad (5)$$

$\sigma_{\text{eff,diff},i}$ is the corresponding width of the gamma distribution of species i . This model was also applied to binary surfactant-water systems, with $x_{\text{if}} = 0$ (e.g., Annunziata et al.^[12]). The two different interfaces must be considered, respectively, for emulsions with semi-crystalline dispersed phases.

Förster et al.^[13] applied the gamma distribution to the modeling of NMR relaxation measurements and found

that the decay of the transverse relaxation of the signal S can be described by

$$S(t) = S_0 \left(1 + t \frac{\sigma_{eff,relax}^2}{\langle R_{2,eff} \rangle} \right)^{-\frac{\langle R_{2,eff}^2 \rangle}{\sigma_{eff,relax}^2}}, \quad (6)$$

where $\langle R_{2,eff} \rangle$ represents the effective transverse relaxation rate, $\sigma_{eff,relax}$ the effective distribution width of relaxation rates of the gamma function, and S_0 the equilibrium signal.

$\langle D_{eff} \rangle$ and $\langle R_{2,eff} \rangle$ in angle brackets are used to directly calculate the effective diffusion coefficient and the effective relaxation rates within the gamma model.

3 | RESULTS AND DISCUSSION

It is unknown so far whether there is a depletion or an accumulation of surfactant molecules at the solid–liquid interface during the crystallization of the droplets. In this work, the surfactant distribution during crystallization of the dispersed phase of organic melt emulsions is investigated by spin–spin relaxation and diffusion measurements of the surfactant molecules. More specifically, we evaluated the ^1H peak of the CH_2 belonging to the polyether chains at the hydrophilic heads of the surfactants. For better readability, we will refer to this peak as the “TW20 peak.” While transverse relaxation measurements dominantly reveal information about the internal and rotational mobility of the surfactant molecules, here of the polyether chains themselves, measurements of the surfactant’s diffusion give insights into their translational movement within the emulsion by diffusion and exchanges between the phases described above. We gain information about the surfactant behavior during droplet crystallization by combining these two NMR techniques.

First, we discuss our results obtained on binary systems (surfactant in water). Second, we discuss our results on emulsions, revealing in-depth insights into the behavior of the surfactant molecules in the O/W emulsion during the crystallization of the dispersed phase.

3.1 | Binary system: TW20 in aqueous solution

First, information about relaxation rates and diffusion coefficients of single surfactant molecules in solution and of molecules in micelles must be gained to explain and interpret the diffusion and relaxation data of the surfactants in an emulsion according to Equations (3) and (4).

Neglecting molecular exchange, we estimate the concentration of surfactant in micelles and as single molecules as follows: It is assumed that no micelles are formed for concentrations below cmc , and the surfactant molecules are present as single surfactant molecules in aqueous solution. At concentrations above cmc , the concentration of the single molecules is equal to cmc , and the micellar surfactant concentration is given by the difference between the total surfactant and the single molecule concentrations (Figure 1).^[14]

The self-diffusion coefficient and relaxation rate for surfactant concentrations below cmc should be independent of the surfactant concentration and should represent the behavior of single molecules. For concentrations above cmc , the effective diffusion coefficient $\langle D_{eff} \rangle$ should decrease with increasing surfactant concentration due to the two different contributions (sm and mic) and exchange between them. The effective relaxation rate should be approximately independent of the surfactant concentration, assuming a constant micellar size and aggregation number. There should not be any spatial obstruction of the molecules themselves, as, according to Basheva et al.,^[15] the aqueous volume fraction of micelles ranged from $2 \cdot 10^{-3}$ to 3.2% ($\tilde{c}_{TW20} = 1.5 \cdot 10^{-2} - 18.6 \text{ mol m}^{-3}$) in our experiments.

Taking preliminary assumptions for the diffusion measurements into account, the steepness of the logarithm of the normalized TW20 signal S/S_0 as a function of q^2 should decrease with increasing surfactant concentration, which is observed in the experiments (Figure 2).

A diffusion time $\Delta = 100 \text{ ms}$ was chosen for all stimulated echo diffusion experiments (Table 2) which is limited by longitudinal relaxation. $\langle T_{1,eff} \rangle$ was measured for binary as well as emulsion systems with liquid droplets and solid particles (Figure S1). $\langle T_{1,eff} \rangle$ was in the range of 300–400 ms and is, therefore, larger than the

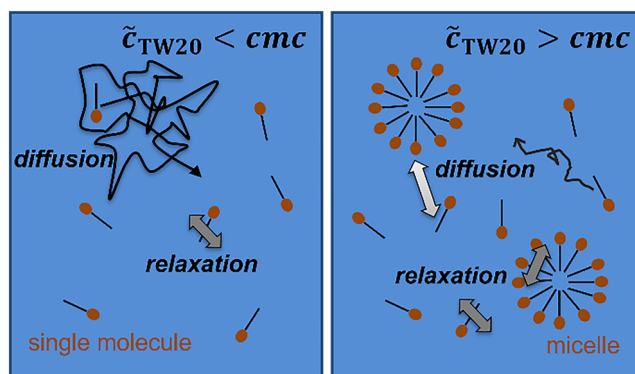


FIGURE 1 Graphical illustration of the surfactant distribution in a binary system of TW20 in water for TW20 concentrations \tilde{c}_{TW20} below (left) and above (right) cmc

chosen Δ . As a result, all species should be observed in the PFG-STE experiments to a large extent. This statement is also supported when taking the initial signal intensity of the diffusion measurements for a range of Δ into account: For $\Delta < 200$ ms, no impact of Δ on S_0 was detectable, whereas S_0 decreased for $\Delta \geq 200$ ms showing the influence of the longitudinal relaxation. These results

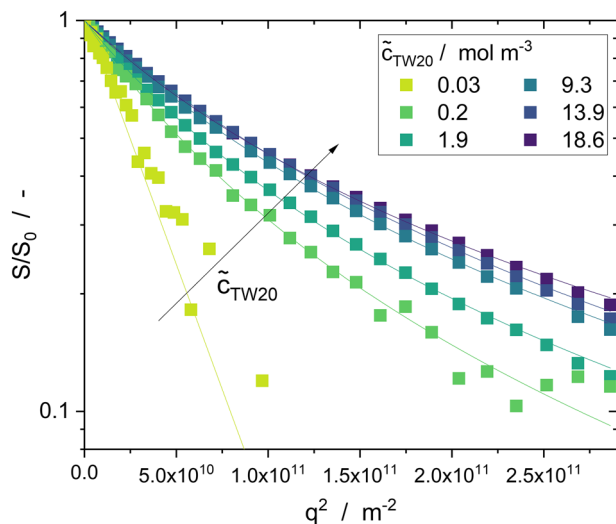


FIGURE 2 PFG-STE signal decay of the TW20 peak (polyether chains, Figure 15) in binary surfactant-D₂O mixtures at different surfactant concentrations. Please note the limited signal-to-noise ratio of the TW20 peak at small concentrations, leading to scattering of the normalized signal at larger q , namely, gradient amplitudes. The lines represent the corresponding gamma fits according to Equation 1. All signal decays have been measured until $S/S_0 \sim 0.05$. For better comparability, they are only shown up to $q^2 \sim 2.8 \cdot 10^{11} \text{ m}^{-2}$.

were the same for binary and emulsion systems with liquid droplets and solid particles.

The gradient duration was constantly $\delta = 2$ ms, and the delay between the two first pulses of the pulsed field gradient stimulated echo (PSF-STE) experiment τ_1 (Figure 17b) was constantly at 5 ms. These times are shorter than the measured transverse relaxation ($< T_{2,eff} > c [40 \dots 300 \text{ ms}]$).

The steepness of the signal decay decreases as a function of q^2 with increasing surfactant concentration. Due to the limited signal-to-noise ratio for measurements below cmc , the determined diffusion coefficients scatter. In addition to the gamma distribution, the Stejskal-Tanner approach^[16] models the experimental data sufficiently well (fit not shown) for surfactant concentrations below cmc . This is because single surfactant molecules are isolated. TW20 additionally has a negligible molecular weight distribution width. Nonetheless, also the Stejskal-Tanner approach leads to a comparable spread of diffusion coefficients for concentrations below cmc . The nonexistence of micelles besides single molecules far below cmc taken from literature^[17] is also reflected in the small distributional width of the gamma function (Figure 3).

In the following, we focus only on the TW20 peak (polyether chains) at 3.65 ppm due to its clear chemical shift separation from other peaks in the spectra and its uniqueness in showing the behavior of the surfactant molecules for both relaxation and diffusion (compare Figure 15).

A faster $< D_{eff} >$ is found at $\tilde{c}_{TW20} < cmc$ compared to the diffusion coefficient above cmc as expected (Figure 3a). For example, $< D_{eff} >$ of sodium dodecyl sulfate depends on the concentration of the surfactant

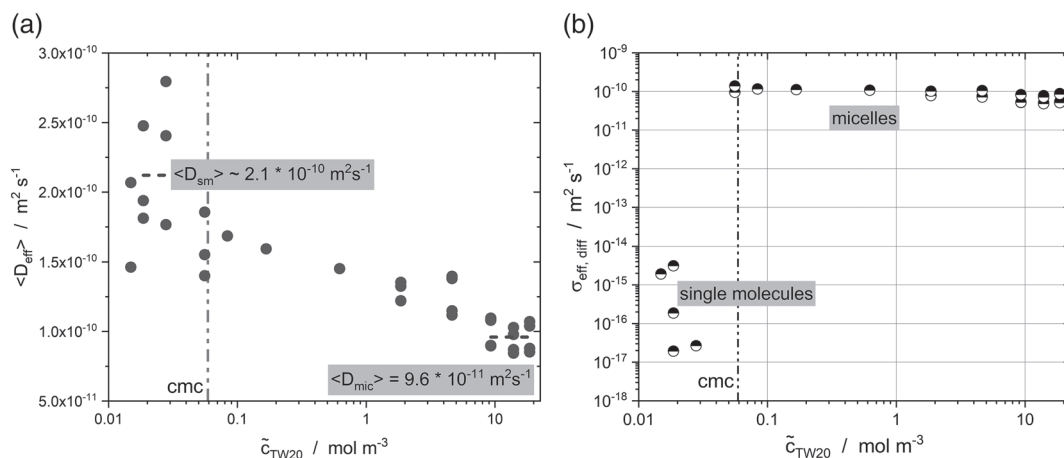


FIGURE 3 (a) $< D_{eff} >$ of TW20 as a function of \tilde{c}_{TW20} in an aqueous solution, dotted line: cmc of TW20 at 298 K ($= 0.059 \text{ mol m}^{-3}$).^[17] (b) The width of the gamma distribution of the diffusion coefficient $\sigma_{eff,diff}$ (Equation 1) as a function of \tilde{c}_{TW20} . $\sigma_{eff,diff}$ is a clear indicator of the occurrence of micelles above the cmc : $\sigma_{eff,diff}$ is significantly larger above cmc .

(see, e.g., Al-Soufi et al.^[18]). $\langle D_{eff} \rangle$ of TW20 in the binary system depends on its concentration up to a surfactant concentration of $\tilde{c}_{TW20} = 9.3 \text{ mol m}^{-3}$. According to Sutherland et al.,^[19] the diffusion coefficient should not change for surfactant concentrations higher than 1 wt % surfactant. This is also visible in our results, as a constant $\langle D_{eff} \rangle$ was found for $\tilde{c}_{TW20} > 10 \text{ mol m}^{-3}$.

The width of the gamma distribution used to model the diffusion data (Figure 3b) increases with increasing \tilde{c}_{TW20} . The scattering of the data for $\tilde{c}_{TW20} < cmc$ is visible for both $\langle D_{eff} \rangle$ and $\sigma_{eff,diff}$, which is due to the small concentrations of the surfactants and the limiting signal-to-noise ratio of the measurements.

A self-diffusion coefficient for single molecules of $\langle D_{sm} \rangle \sim 2.1 \cdot 10^{-10} \text{ m}^2 \text{ s}^{-1}$ ($T = 289 \text{ K}$) was calculated by averaging the determined, scattered diffusion coefficients for $\tilde{c}_{TW20} < 0.04 \text{ mol m}^{-3}$. We will discuss later that the cmc is not one exact given concentration but there is a range around the cmc where micelles can be formed as well. Therefore, we use a concentration smaller than the cmc to ensure only taking single molecules into account.

Equation (3) with $x_{if} = 0$ is used to calculate the self-diffusion coefficient of micelles. By doing so, the effective mean self-diffusion coefficient of the micelles is found to be $\langle D_{mic} \rangle = 9.6 \cdot 10^{-11} \text{ m}^2 \text{ s}^{-1}$ for concentrations up to $\tilde{c}_{TW20} \leq 18.6 \text{ mol m}^{-3}$ at $T = 289 \text{ K}$. Lushtinetz and Dosche^[20] determined micellar diffusion coefficients of $7.5 - 7.9 \cdot 10^{-11} \text{ m}^2 \text{ s}^{-1}$ in aqueous systems for TW20 surfactant concentrations between 0.1 and 10 mol m^{-3} at $T = 294 \pm 0.5 \text{ K}$. Mandal et al.^[21] calculated diffusion coefficients of TW20 micelles above cmc to $7.76 \cdot 10^{-11} \text{ m}^2 \text{ s}^{-1}$ ($T = 298 \text{ K}$). Carnero Ruiz et al.^[22] published a diffusion coefficient of $9.25 \cdot 10^{-11} \text{ m}^2 \text{ s}^{-1}$ ($T = 298 \text{ K}$) for $4.1 \text{ mol m}^{-3} < \tilde{c}_{TW20} < 20.4 \text{ mol m}^{-3}$, measured by light scattering. These values agree with our findings. Hildebrandt et al.^[23] observed a constant diffusion coefficient for the phospholipids below the cmc , followed by a decrease of the diffusion coefficient with increasing phospholipid concentrations (above cmc). This is also visible for our diffusion coefficients of TW20 for $0.06 \text{ mol m}^{-3} < \tilde{c}_{TW20} < 6 \text{ mol m}^{-3}$.

Using the Stokes-Einstein equation,^[24] micellar diameters can be estimated to be approximately 4 nm from $D_{mic} = 9.6 \cdot 10^{-11} \text{ m}^2 \text{ s}^{-1}$ ($T = 289 \text{ K}$, dynamic viscosity of the binary system $\eta_{TW20,D_2O} = 1.1 \cdot 10^{-3} \text{ Pa s}$ and the Boltzmann constant $k_B = 1.380649 \cdot 10^{-23} \text{ J K}^{-1}$). Additional and independent small-angle X-ray scattering (SAXS) measurements led to an average micellar radius of approximately 5.0 nm at a $\tilde{c}_{TW20} = 18.4 - 23.1 \text{ mol m}^{-3}$ at 293 K. No difference in micellar size was observed in the SAXS measurements in the samples regarding the initial surfactant concentration. Moreover, these results

are in good agreement with micellar diameters estimated from our diffusion measurements and data presented in literature (^[25]: 4.5 nm, ^[15]: 7.2 nm).

$cmc = 0.059 \text{ mol m}^{-3}$ (Figure 3) was determined at 298 K in Linke.^[17] Using temperature-dependent data of cmc measured by means of interfacial tension,^[22] $cmc = 0.073 \text{ mol m}^{-3}$ can be calculated at $T = 289 \text{ K}$ by interpolating the given data. Figure 3 points out that there is not a sharp transition in $\langle D_{eff} \rangle$, but a clear difference is visible for $\sigma_{eff,diff}$. According to our measurements, we therefore estimate cmc to be between $\tilde{c}_{TW20} = 0.028 \text{ mol m}^{-3}$ and $\tilde{c}_{TW20} = 0.056 \text{ mol m}^{-3}$ at $T = 289 \text{ K}$. The existence of a transition zone around cmc where micelles are not yet fully stable is also mentioned in literature.^[26]

In addition, the signal decays (Figure 2) do not show two distinct regions in steady state for $\tilde{c}_{TW20} > cmc$, which would be expected for two independently occurring species. The smooth transition and the need to model the data by a monomodal distribution indicate, however, a fast exchange of molecules between the species “single molecule” and “micelle.”

The intrinsic, molecular mobility of the hydrophilic surfactants' head groups (TW20 peak due to the CH_2 in the polyether chains, peak at 3.65 ppm in the ^1H spectra, Figure 15) was investigated by transverse relaxation measured via the Carr-Purcell-Meiboom-Gill (CPMG) pulse sequence^[27] (Figure 4). The magnetization decays of the relaxation measurements were modeled according to equation (6). We find the coefficient of determination to be larger than $R^2 > 0.96$ for all fits. All signal decays were measured up to $\left(\frac{S}{S_0}\right)_{relax} \sim 0.05$. The signal-to-noise ratio limited the measurement accuracy especially for $\tilde{c}_{TW20} < cmc$.

A transverse relaxation rate $\langle R_{2,sm} \rangle$ around 3.0 s^{-1} was measured for single molecules at $\tilde{c}_{TW20} < cmc$. $\langle R_{2,eff} \rangle$ gradually increased with increasing surfactant concentration as micelles were formed. An approximately constant $\langle R_{2,eff,mic} \rangle$ of 4.5 s^{-1} was observed for surfactant concentrations larger than 1.9 mol m^{-3} . It becomes obvious that there is an impact of single molecules on the relaxation measurements in binary systems for $\tilde{c}_{TW20} > cmc$ and $< 1.9 \text{ mol m}^{-3}$. This observation is the basis for the usage of Equations (3) and (4) and for the interpretation of relaxation rates. Like $\sigma_{eff,diff}$, also $\sigma_{eff,relax}$ can be exploited to differentiate the two states of the molecules: single molecules and micelles. According to the Tukey test, the mean values of the two populations (sm , mic) are significantly different at a level of 0.05.

Platz^[28] found an analogous curve of the relaxation rates for the methyl group of the surfactant sodium dodecyl sulfate. To the best of our knowledge, no other

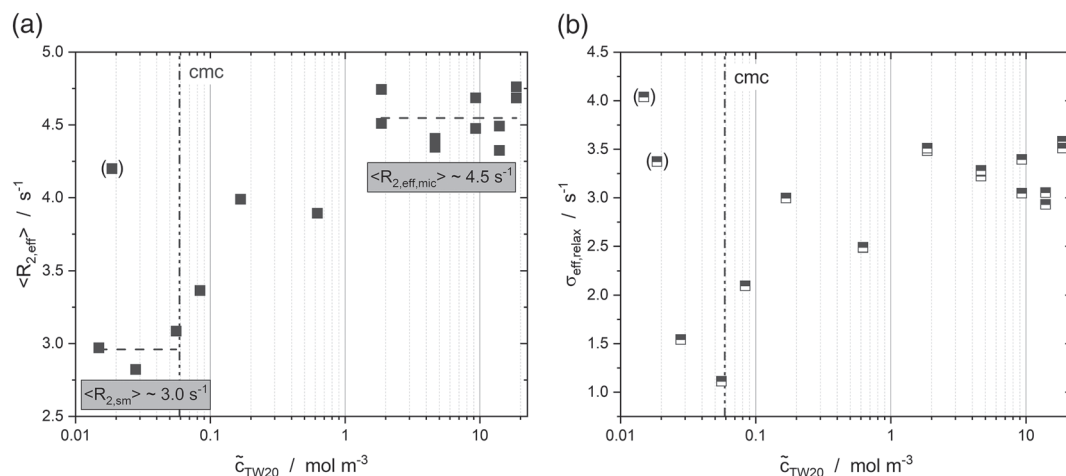


FIGURE 4 (a) The effective transverse relaxation rate $\langle R_{2,eff} \rangle$ of TW20 (polyether chains) and (b) the corresponding width of the gamma distribution $\sigma_{eff,relax}$ (Equation 6) as a function of the surfactant concentration \tilde{c}_{TW20} . $\langle R_{2,sm} \rangle$ and $\langle R_{2,eff,mic} \rangle$ represent the (effective) transverse relaxation rates of the single molecules and micelles, respectively.

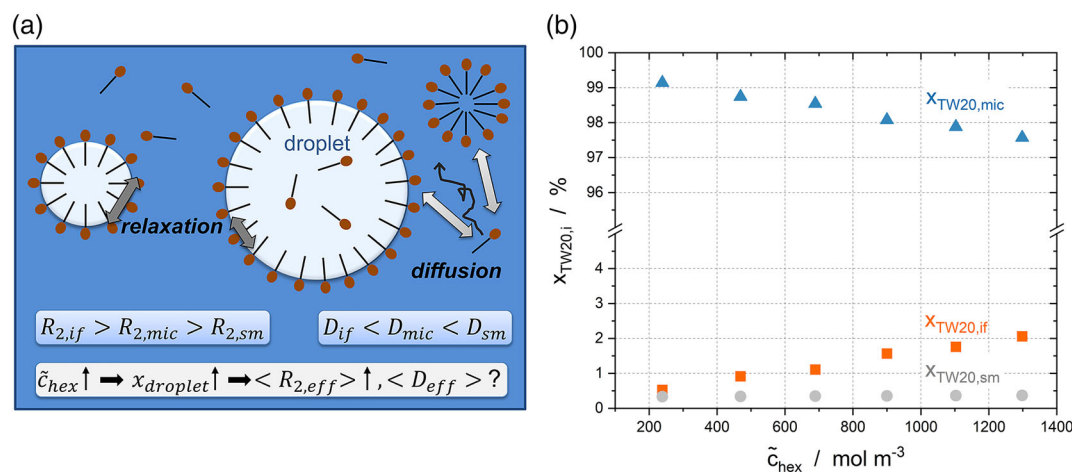


FIGURE 5 (a) Graphical abstraction of the surfactant in emulsions with liquid–liquid interfaces. The expected changes in $\langle R_{2,eff} \rangle$ and $\langle D_{eff} \rangle$ when changing \tilde{c}_{hex} are indicated. (b) Calculated relative surfactant fractions in the three states of the surfactants (single molecules, micelles, and at the interfaces).

comparable relaxation studies of the surfactants have been done for micellar systems, emulsions, or suspensions so far.

3.2 | Diffusion and relaxation of emulsions (liquid–liquid interfaces)

Creaming of the emulsion must be negligible during the measurement time to study the emulsions reliably (see Supporting Information S2): Approximately 5% of the dispersed phase underwent creaming within the relevant time scales of the diffusion and relaxation measurements (8.5 and 18.5 min). As only 5% of the signal was lost due to creaming, this process and loss will be neglected in

further data analysis. We will show later that the signal loss is much larger (up to 75%) due to relaxation phenomena during the NMR experiment, for example, between excitation and signal acquisition.

Different n-hexadecane concentrations were studied at $\tilde{c}_{TW20} = 16\text{--}18 \text{ mol m}^{-3}$ to investigate the effect of the interface in emulsions. The mean volume-based droplet diameter increased from 2.7 to 3.4 μm with increasing n-hexadecane concentrations ($\tilde{c}_{hex} = 239\text{--}1,298 \text{ mol m}^{-3}$), whereas the distribution width of the DSD decreased (Figure S3).

There are two possible findings for the TW20 diffusion on emulsion systems with liquid–liquid interfaces (Figure 5):

1. Considering the increasing amount of surfactant at the droplet interfaces and slightly decreasing micelles concentrations with increasing n-hexadecane fractions, a smaller value of $\langle D_{eff} \rangle$ of TW20 may be expected.
2. A constant $\langle D_{eff} \rangle$ may be expected if the contributions either of micelles or surfactant molecules at the liquid-liquid interface are dominant. The sum of all the other diffusion coefficients of the existing species will then be dominated by the respective value of the dominating species.

We will start with the diffusion measurements (Figure 6) and combine the gained results with the relaxation experiments (Figure 7) in the following.

$\langle D_{eff} \rangle$ was found to be almost independent of \tilde{c}_{hex} for $\tilde{c}_{hex} < 700 \text{ mol m}^{-3}$ (Figure 6) when using Equation (1) to describe the measured range of $q^2 \leq 2.6 \cdot 10^{12} \text{ m}^{-2}$. $\sigma_{eff,diff}$ increased slightly with \tilde{c}_{hex} . $\langle D_{eff,avg} \rangle = 8.6 \cdot 10^{-11} \text{ m}^2 \text{ s}^{-1}$ is slightly smaller than the self-diffusion coefficient of micelles ($\langle D_{mic} \rangle = 9.6 \cdot 10^{-11} \text{ m}^2 \text{ s}^{-1}$). This indicates that a portion of the surfactant molecules belongs to larger moieties compared to the moieties in the binary system, which should be represented by the added interface.

Guan et al.^[29] and Bernewitz et al.^[30] found decreasing diffusion coefficients of water molecules when increasing the fraction of the dispersed phase. Taking the signal decays for $q^2 < 1.0 \cdot 10^{12} \text{ m}^{-2}$ into account (Figure S4), we also find slower $\langle D_{eff} \rangle$ of the surfactants' polyether chains at the hydrophilic head groups

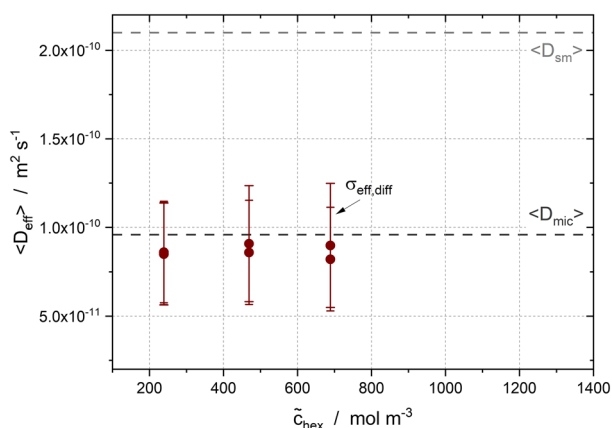


FIGURE 6 The effective diffusion coefficient $\langle D_{eff} \rangle$ for the head group of TW20 is constant at an n-hexadecane concentration $\tilde{c}_{hex} < 700 \text{ mol m}^{-3}$. The corresponding width of the gamma distribution $\sigma_{eff,diff}$ (Equation 1) is shown as “error bars.” All concentrations were measured twice. The lines at $\langle D_{mic} \rangle$ and $\langle D_{sm} \rangle$ represent the self-diffusion coefficients of TW20 micelles and TW20 single molecules, respectively.

with increasing dispersed phase fractions. The dispersed phase hinders surfactant diffusion due to an increasing number of phase boundaries. Not all molecules can adsorb at the interphases, and, consequently, an increasing fraction is hindered in terms of lower mean displacement within the diffusion time defined in the NMR experiment.

$\langle R_{2,eff} \rangle$ of the head groups is expected to increase with increasing droplet size, and, consequently, increasing \tilde{c}_{hex} should lead to shorter transverse relaxation times. The latter is due to the reduction of the radius of curvature with increasing droplet size, leading to a higher interference of the molecules' head groups with each other (Figures 5 and 7).

This expectation is observed in the measurements of transverse relaxation: Increasing \tilde{c}_{hex} led to larger $\langle R_{2,eff} \rangle$ and $\sigma_{eff,relax}$ of the head group of TW20 (Figure 7). Compared to the binary solution, the relaxation rates increase from $\langle R_{2,sm} \rangle \sim 3 \text{ s}^{-1}$ and $\langle R_{2,eff,mic} \rangle \sim 4.5 \text{ s}^{-1}$ to values roughly between 10 s^{-1} and 20 s^{-1} , respectively. $\langle R_{2,eff,mic} \rangle$ fits well to the approximately linear relation between $\langle R_{2,eff} \rangle$ and \tilde{c}_{hex} in the concentration regime investigated.

For solid-like systems, the main relaxation path for ^1H measurements is the homonuclear dipolar interaction. The relaxation rates (transverse and longitudinal) are basically described by the squared interaction and the corresponding spectral densities. For the latter, a Lorentz form can be assumed in the simplest case (see, e.g., Abragam^[31]). The longitudinal relaxation

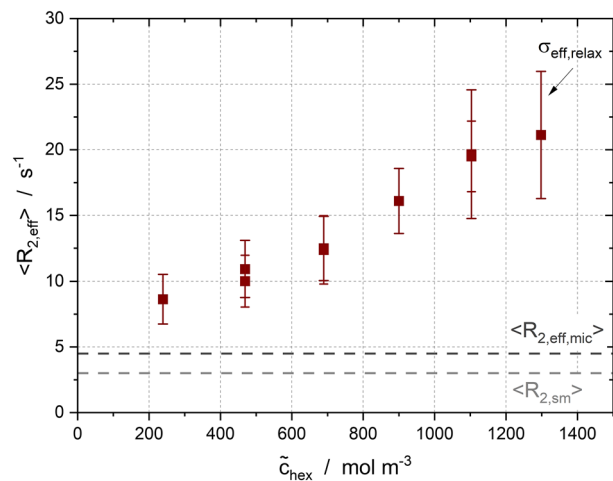


FIGURE 7 $\langle R_{2,eff} \rangle$ of the head group of TW20 as a function of dispersed phase concentration. The corresponding width of the gamma distribution $\sigma_{eff,relax}$ (according to Equation 6) is shown as “error bars.” All concentrations were measured twice. Both values increase with \tilde{c}_{hex} . $\langle R_{2,eff,mic} \rangle$ and $\langle R_{2,sm} \rangle$ represent the effective relaxation rate the head group of TW20 in micelles and as single molecules, respectively.

depends on intermolecular and intramolecular interactions. The intramolecular interactions rely on the motional correlation time τ_c ($\tau_c \uparrow \rightarrow R_2 \downarrow$), whereas for the intermolecular interactions, also, the distance between the various molecules r plays a role ($r \uparrow \rightarrow R_2 \downarrow$).

Transferring Equation (3) to relaxation measurements, the effective mean relaxation rate of the molecules at the liquid–liquid interface $\langle R_{2,eff,if} \rangle$ increased with \tilde{c}_{hex} , indicating, in a simple picture, either decreased motional correlation times or decreased distances between the head groups of TW20 at the liquid–liquid interface. Both could depict that the surfactant molecules' head groups are more structured at the interface with increasing droplet sizes. This is in accordance with the decreasing radius of curvature of the surface with increasing droplet sizes and verifies our hypothesis stated earlier.

The relaxation and diffusion investigations with differing dispersed phase concentrations and droplet sizes of the emulsions led to the conclusion that the surfactant molecules are influenced by the phase boundaries and, additionally, transverse relaxation measurements can be used to investigate the interfacial surfactant molecules.

3.3 | Diffusion and relaxation of emulsions and suspensions (with liquid–liquid and liquid–solid interfaces)

3.3.1 | Liquid–liquid interfaces

The surfactant concentration was varied at a constant dispersed fraction of $\tilde{c}_{hex} \sim 900 \text{ mol m}^{-3}$ to investigate whether the droplets and particles are surrounded by a

monolayer or even a multilayer of surfactant molecules. Additionally, the dispersed phase of these emulsions was (partly) crystallized to investigate the surfactant distribution while varying the solid dispersed phase fractions.

The expectations are summarized in the following:

- $\langle R_{2,eff} \rangle$ should be independent of \tilde{c}_{TW20} , if $\tilde{c}_{TW20} > cmc$ and $\tilde{c}_{TW20,if} = \text{const.}$
- An increase in the packing density of the surfactants at the interface should lead to an increasing $\langle R_{2,eff} \rangle$, complementary to the observations in Figure 7.
- $\langle D_{eff} \rangle$ of TW20, in combination with $\sigma_{eff,diff}$, should decrease only slightly with increasing numbers of surfactant molecules at the interface as we noticed earlier that the measured diffusion is dominated by the micellar diffusion (Figures 8 and 9).

In addition, the question about the mean residence time in the specific environments has to be considered. The expectations above are formulated for three independent compartments where the surfactants could be presented.

$\langle R_{2,eff} \rangle$ of TW20 is almost constant for the fresh, completely liquid emulsion. $\langle D_{eff} \rangle$ of TW20 decreases only slightly with increasing surfactant concentration.

Divergent results regarding the number of surfactant molecules at the interface are reported in the literature: Increasing interfacial surfactant coverages with increasing total surfactant concentrations, for example, were reported by Penfold et al.^[32] for ethoxylated polysorbate nonionic surfactants at the n-hexadecane–water interface for the concentration range up to $\tilde{c}_{surfactant} = 3 \text{ mol m}^{-3}$. On the contrary, Brinck et al.^[33] did not measure any further increase of the surfactant numbers at the liquid–

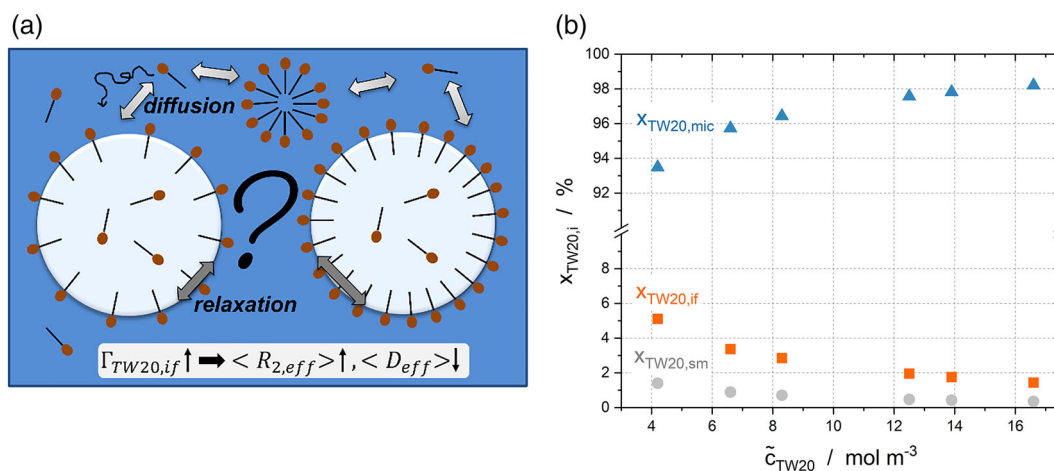


FIGURE 8 (a) Graphical illustration of two possible coverages of the droplets' interfaces with surfactant molecules $\Gamma_{TW20,if}$, which may occur due to an increased overall surfactant concentration. An increase in the interfacial coverage should lead to an increase of $\langle R_{2,eff} \rangle$ and a decrease of $\langle D_{eff} \rangle$. (b) Calculated relative surfactant concentration in the three different environments (*sm*, *mic*, and *if*)

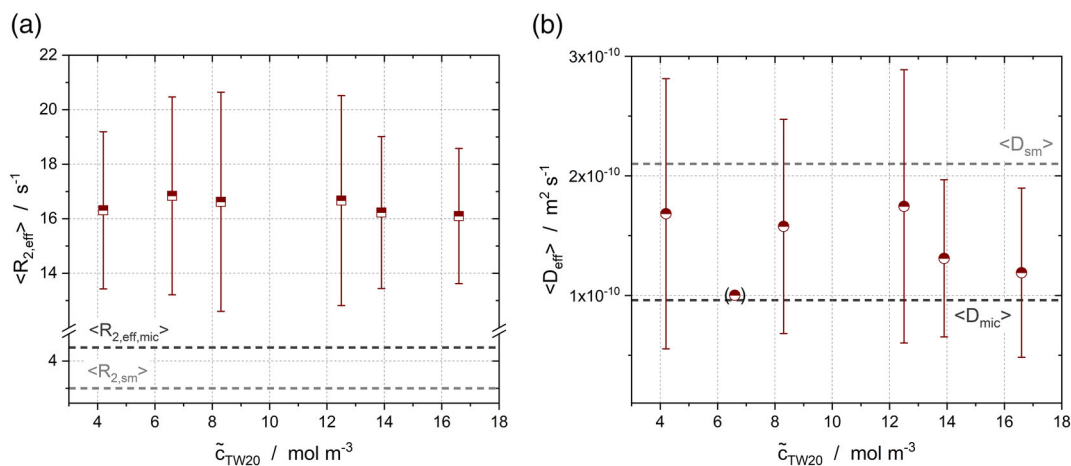


FIGURE 9 Effective relaxation rates (a) and effective diffusion coefficients (b) of the polyether chains of TW20 (TW20 peak) in the O/W emulsions with varying surfactant concentrations at $T = 289$ K with $\tilde{c}_{hex} \sim 900$ mol m^{-3} . Additionally, the distribution width of the corresponding gamma distribution is shown in form of “error bars.” $\langle R_{2,eff,mic} \rangle$ and $\langle R_{2,sm} \rangle$ represent the effective relaxation rate of the head group of TW20 in micelles and as single molecules, respectively, and $\langle D_{mic} \rangle$ and $\langle D_{sm} \rangle$ indicate the self-diffusion coefficients of TW20 micelles and single molecules.

liquid interface when cmc was exceeded. The latter would be following our measurements, assuming that the accuracy and sensitivity of the measurements were not a limitation, while the slight decrease in $\langle D_{eff} \rangle$ (in combination with the given $\sigma_{eff,diff}$ and visible also in the raw signal decays) gives an indication of an increasing number of micellar moieties.

3.3.2 | Liquid–liquid and solid–liquid interfaces

Besides determining the solid fraction of n-hexadecane from the spectroscopic measurements, 1H spectra were analyzed regarding the TW20 peak (polyether chains, cf. Figure 15) (Figure 10).

The integral of the TW20 peak $(A_{TW20})_{spec}$, which corresponds to the polyether chains at the surfactants' head groups, did not change as a function of ξ_{hex} . Thus, the head groups of these surfactants, which were bound to the solid–liquid interface, remained mobile on the time scale of the spectroscopic measurements. Also, the line width, as well as the signal amplitude, did not change as a function of ξ_{hex} . No statement can be made for the tail of the surfactant as the signal was overlaid by the n-hexadecane signal. Exemplarily, two TW20 peaks are shown in Figure 15 in Section 5 for different ξ_{hex} .

Relaxation thus should reflect the state of the head groups independent of the aggregation state of the droplet (solid or liquid) as long as the interfacial coverage stays constant. Substances, such as surfactant molecules, can also be released from the droplet during

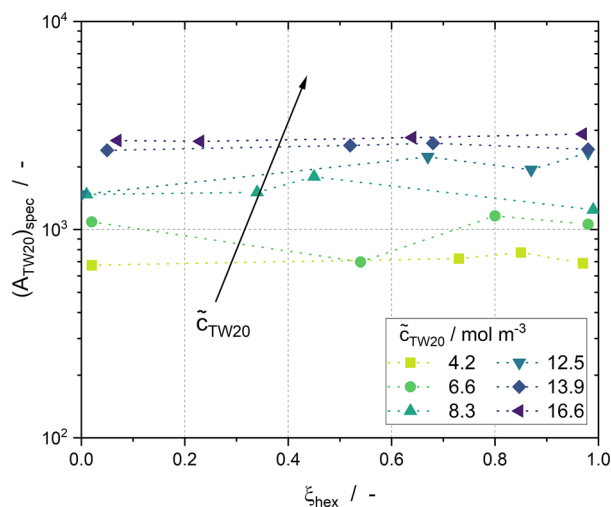


FIGURE 10 The integral of the TW20 peak $(A_{TW20})_{spec}$, representing the detected number of head groups of TW20, stays approximately constant as a function of the solid fractions of the dispersed phase.

crystallization. This would increase the translational mobility also of the remaining interfacial molecules, decrease the interfacial coverage, and, consequently, increase the surfactant concentration in the aqueous phase. All mentioned aspects would correspond to a decrease in relaxation rate (Figure 11).

We start with the discussion of the relaxation measurements (Figure 12), followed by the interpretation of the diffusion measurements (Figure 13). The influence of the echo time τ_{echo} on $\langle R_{2,eff} \rangle$ has to be considered; thus, experiments with $\tau_{echo} \in [0.4\text{--}6$ ms] were carried out. The initial signal amplitudes $(S_{0,TW20})_{relax}$ were

independent on τ_{echo} . The signal decay, therefore, contains all the moieties present in the system as long as the transverse relaxation is larger than 0.4 ms. Contributions of the exchange on $\langle R_{2,eff} \rangle$ are neglected in a first interpretation of the data.

$\langle R_{2,eff} \rangle$ of the observed fraction of TW20 head groups decreased (Figure 12a) with increasing solid fraction of the dispersed phase of an O/W emulsion with $\tilde{c}_{hex} \sim 900 \text{ mol m}^{-3}$ (at 289 K, increasing ξ_{hex}), reaching a value of about 8 s^{-1} , which is approximate twice the value of $\langle R_{2,eff,mic} \rangle$.

It may be possible that the transverse relaxation of the molecules at the solid–liquid interface is so fast that the magnetization of that phase was not acquired. This aspect can be addressed by considering the extrapolated

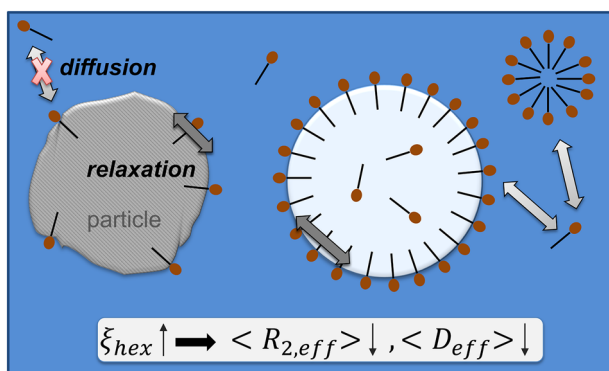


FIGURE 11 Graphical abstraction of the surfactant distribution in the emulsion during crystallization of the dispersed phase at a constant temperature of $T = 289 \text{ K}$. The expected result of an increasing solid fraction of the dispersed phase on both, relaxation and diffusion, is additionally given.

magnetization amplitude ($(S_{0,TW20})_{relax}$ (Figure 12b): No significant change in the signal intensity measured at $T = 289 \text{ K}$ was observed for $\xi_{hex} < 0.7$.

No dependency between $(S_{0,TW20})_{relax}$ and ξ_{hex} ($\xi_{hex} < 0.7$)

As $\langle R_{2,eff} \rangle$ already decreases for $\xi_{hex} < 0.7$, this corresponds with either an increasing τ_c and/or an increase of r . Both would lead to the interpretation that surfactant molecules detach from the interface during crystallization. Consequently, the particles have a smaller number of surfactant molecules at their interfaces compared to the liquid–liquid droplet interface.

Dependency between $(S_{0,TW20})_{relax}$ and ξ_{hex} ($\xi_{hex} > 0.7$)

For $\xi_{hex} > 0.7$, the differences of $(S_{0,TW20})_{relax}$ from the initial $(S_{0,TW20})_{relax}$ ($\xi_{hex} = 0$) amounts to roughly an order of magnitude. This large difference cannot only be explained by signal loss due to surfactant molecules frozen to the solid–liquid interface: Only between about 5% ($\tilde{c}_{TW20} = 4.2 \text{ mol m}^{-3}$) and 1.5% ($\tilde{c}_{TW20} = 16.6 \text{ mol m}^{-3}$) of the total surfactant concentration is adsorbed to the liquid–liquid interface (assuming an interfacial surfactant coverage of $\Gamma_{TW20,if} = 3.62 \cdot 10^{-6} \text{ mol m}^{-2}$).^[34] Therefore, another mechanism must lead to the signal reduction. It may be assumed that n-hexadecane molecules could also be found within micelles or nanodroplets, which represent the largest portion of surfactant molecules compared to the two other states (*sm* and *if*).

Weiss et al.^[35] and Dungan et al.^[36] reported material transport between dispersed droplets due to the integration of n-hexadecane molecules into TW20 micelles. SAXS measurements showed that the micellar form

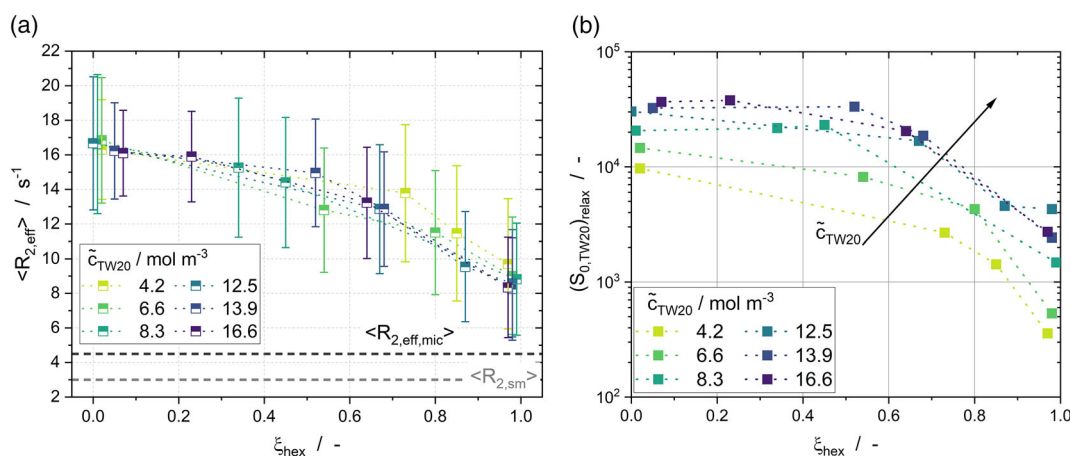


FIGURE 12 (a) $\langle R_{2,eff} \rangle$ measured at $T = 289 \text{ K}$ for varying solid fractions of the dispersed phase at the indicated surfactant concentrations with $\tilde{c}_{hex} \sim 900 \text{ mol m}^{-3}$. The “error bars” represent $\sigma_{eff,relax}$ (Equation 6). (b) $(S_{0,TW20})_{relax}$, the signal intensity of the CPMG extrapolated to zero echo time, was obtained from the fit of the gamma distribution model. A significant signal loss is observed for $\xi_{hex} > 0.7$ and needs to be considered in data interpretation.

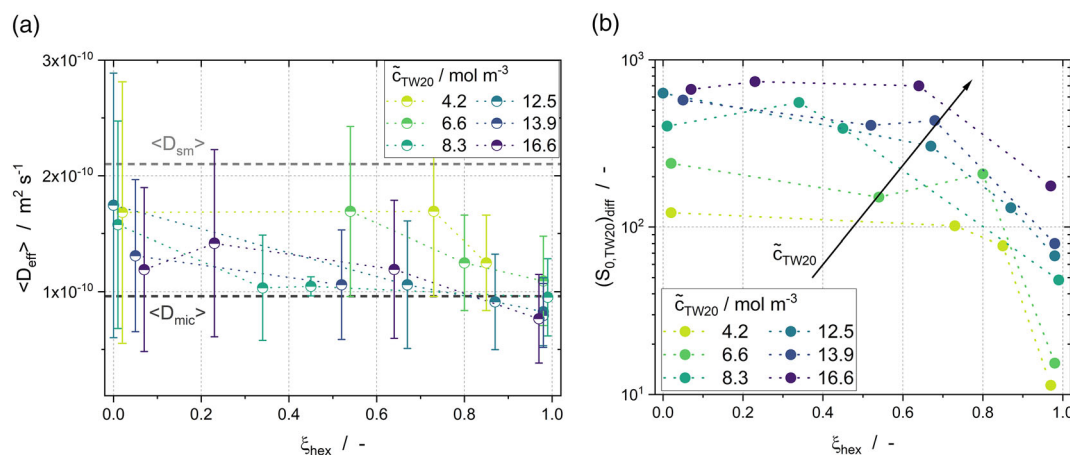


FIGURE 13 (a) $\langle D_{eff} \rangle$ of O/W emulsions at $T = 289 \text{ K}$ as a function of ξ_{hex} for different surfactant concentrations. The “error bars” represent $\sigma_{eff,diff}$ according to Equation 1. (b) $(S_{0,TW20})_{diff}$, the PFG-STE signal intensity extrapolated to $g = 0 \text{ T m}^{-1}$, shows an overall similar behavior as found in transverse relaxation measurements (Figure 12).

differed between the native state in binary systems and the state when the micelles were previously part of the emulsion and, therefore, exposed to n-hexadecane molecules. As mentioned in the experimental section, the slope of the signal intensity at small q -vectors in SAXS experiments tended to be larger in the presence of n-hexadecane. In addition, an increased layer thickness of approximately 0.5 nm for those micelles was found when using the Bragg equation. Therefore, the signal loss observed in the relaxation measurements could be due to the decreased mobility of surfactant molecules in these larger micelles or nanodroplets. Another possibility would be that multilayer micelles were formed with reduced mobility of inner TW20 head groups due to polar interaction, resulting in a more regular orientation of the head groups.

El Rhafiki et al.^[37] determined that monodispersed n-hexadecane droplets of 10 nm in diameter need a subcooling of approximately $\Delta T \sim 13 \text{ K}$ to crystallize. In the present work, a subcooling of $12.6 \text{ K} \pm 1 \text{ K}$ was used to increase ξ_{hex} , leading to the explanation that the changes in $S_{0,TW20}$ are due to the crystallization of nanometer-sized droplets (micelles with n-hexadecane inside). Although all our measurements were done at 289 K, thawing of the crystallized structures is not probable, as the melting temperature of n-hexadecane of 291 K was not exceeded. These findings support the immobilization of surfactant molecules at the liquid–solid interface of micrometer- and nanometer-sized droplets.

As a result of the loss of S_0 , we assume most of these surfactants that are bound to solid–liquid interfaces (frozen droplets or nanodroplets) are no longer measurable. This leads to a decrease of $\langle R_{2,eff} \rangle$ and can explain why $\langle R_{2,eff} \rangle \rightarrow \langle R_{2,eff,mic} \rangle$ for $\xi_{hex} \rightarrow 1$. In combination

with the detachment of surfactant molecules from the interface, the relative fraction of the single molecules and simple micelles increases, leading to the observed decrease of $\langle R_{2,eff} \rangle$ as a function of ξ_{hex} .

Taking previously stated findings into account, the measurable range of diffusion coefficients (combination of $\langle D_{eff} \rangle$ and $\langle \sigma_{eff,diff} \rangle$) should be in line with the data for micelles for $\xi_{hex} \rightarrow 1$. As we noticed earlier, there is a signal loss for $\xi_{hex} > 0.7$, which leads to the fact that molecules at interfaces can hardly be detected anymore (Figure 13).

No dependency between $(S_{0,TW20})_{diff}$ and ξ_{hex} ($\xi_{hex} < 0.7$)

The signal intensity at $g = 0 \text{ T m}^{-1}$, $(S_{0,TW20})_{diff}$, and $\langle D_{eff} \rangle$ stayed approximately constant for $\xi_{hex} < 0.7$, whereas $\sigma_{eff,diff}$ (shown as ‘error bars’) decreased with increasing ξ_{hex} . If surfactant molecules at interfaces diffuse with the diffusion coefficient of the droplet or particle, the latter should exhibit a similar size. This is because there should not be a difference in the size of the particles and the droplets. Therefore, the change in the range of the measurable diffusion coefficients might be explained by the prevention of any further exchanges between surfactant molecules bound to the solid–liquid interface and single molecules in the continuous phase, compared to those located at the liquid–liquid interface.

Biswal and Singh^[38] determined the apparent diffusion coefficient of TW20 $D_{a,TW20}$ for the adsorption to an n-hexane- D_2O interface at surfactant concentrations above cmc by pendant drop tensiometry. They found increasing $D_{a,TW20}$ for increasing aqueous surfactant concentrations in the range of $D_{a,TW20} \sim 1.6\text{--}2.4$

$10^{-9} \text{ m}^2 \text{ s}^{-1}$ ($\tilde{c}_{TW20} = 0.01\text{--}0.1 \text{ mol m}^{-3}$). A molecular exchange of water in double emulsions was shown previously by Guan al.^[29] by PFG-STE-NMR. Consequently, a surfactant exchange is likely for emulsions with liquid dispersed phases, leading to the faster $\langle D_{eff} \rangle$ of TW20 in combination with a wider $\sigma_{eff,diff}$ compared to emulsions where the surfactant molecules are bound to the interfaces. In the latter case, molecular exchange may be slowed down or completely neglectable. The exchange of surfactant molecules in systems with liquid interfaces probably shows up in the bending of the signal decay curve at smaller gradient amplitudes (Figure S4, $q^2 < 10^{11} \text{ m}^{-2}$).

Dependency between $(S_{0,TW20})_{diff}$ and ξ_{hex} ($\xi_{hex} > 0.7$)

At $\xi_{hex} > 0.7$, the initial signal intensity decreases with increasing ξ_{hex} by a factor of approximately 10. The first echo of the diffusion measurement was always measured at 101 ms after magnetization excitation. Compared to the spectroscopic measurements ($\Delta t_{dead\ time} = 6.5 \text{ }\mu\text{s}$, probe: DiffBB) and to CPMG ($\tau_{echo} = 4 \text{ ms}$), fast-relaxing spins are only measurable to a low extent after roughly 101 ms. In contrast to the CPMG, where only transverse relaxation takes place, longitudinal relaxation also must be considered in PFG-STE experiments. The dominant mechanism for signal attenuation is transverse relaxation. Together with the possible decrease in the interfacial exchanges, the decrease of $\langle D_{eff} \rangle$ and $\sigma_{eff,diff}$ may represent the increasing number of micelles and nanometer-sized droplets with increasing surfactant concentration when considering those surfactant molecules at the frozen larger droplets interfaces are almost undetectable for $\xi_{hex} > 0.7$.

Taking all experimental results and interpretations into account, the following statements about the surfactant can be made (Figure 14).

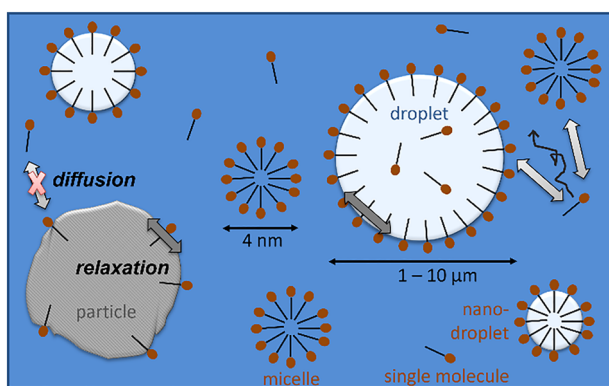


FIGURE 14 Graphical illustration of the surfactant behavior and distribution within an organic O/W emulsion with a semi-crystalline dispersed phase

- Exchange is possible between surfactant molecules in the aqueous phase and at the liquid–liquid interfaces. With the crystallization of the droplet, the interfacial exchange might be diminished.
- In addition to micelles and micrometer-sized droplets, nanometer-sized droplets (= micelles with organic phase inside) can also be found.
- During the crystallization of the droplets, surfactant molecules detach from the interfaces, decreasing the interfacial surfactant coverage.

4 | CONCLUSION

The NMR measurements allowed us to investigate the distribution of surfactant molecules in O/W emulsions during the crystallization of the dispersed phase of an exemplarily n-hexadecane-in-water emulsion.

The solid fraction of the dispersed phase was measured in-situ via NMR spectroscopy, and the crystallization progress could be monitored. Moreover, the spectra revealed the new insight that the polyether chains of the surfactant head groups did not freeze completely at the solid particle surface as their ^1H signal was measured over the temperatures and time ranges without losses.

Diffusion and relaxation measurements of binary D_2O -surfactant systems revealed a mean self-diffusion coefficient for single TW20 molecules of $\langle D_{sm} \rangle \sim 2.1 \cdot 10^{-10} \text{ m}^2 \text{ s}^{-1}$ and an average self-diffusion coefficient for TW20 micelles of $\langle D_{mic} \rangle = 9.6 \cdot 10^{-11} \text{ m}^2 \text{ s}^{-1}$ (both at $T = 289 \text{ K}$). The (effective) mean relaxation rate of the head group of a single molecule was determined to $\langle R_{2,sm} \rangle = 3.0 \text{ s}^{-1}$ and of micelles to $\langle R_{2,eff,mic} \rangle = 4.5 \text{ s}^{-1}$. Moreover, the measurements on binary systems allowed for the conclusion that the relaxation rate can be seen as a combination of the relaxation of the appearing moieties. TW20 micelles were found to have a diameter of approximately 4.0 nm.

An increase in the mean droplet size of emulsions with liquid–liquid interfaces led to increasing motional correlation times and distances between the surfactant molecules at the interface. An increasing surfactant concentration did not lead to an increase in the interfacial surfactant coverage or the formation of an interfacial multilayer. For the first time, we could prove for solid–liquid interfaces that the surfactant molecules detached from the interface, leading to lower interfacial surfactant loadings of crystalline particles compared to the liquid droplets. Moreover, the exchange of the surfactant molecules between the solid–liquid interface and the

aqueous phase might be hampered. N-hexadecane molecules were found to be in some of the nanometer-sizes micelles, which can also crystallize.

5 | EXPERIMENTAL

5.1 | Preparation of emulsions and binary systems

A ternary system of n-hexadecane (Hexadecane ReagentPlus[®], 99%, Sigma-Aldrich, St. Louis, Missouri, United States), deuterium oxide (D₂O, 99.9 atom-% D, Sigma-Aldrich, St. Louis, Missouri, United States) and polysorbate 20 (Tween[®]20, Merck KGaA, Darmstadt, Germany) was prepared as O/W model emulsion system. The aqueous continuous phase was D₂O and the nonaqueous dispersed phase was n-hexadecane. The surfactant TW20 stabilized the dispersed phase. TW20 is a well-characterized surfactant with a *cmc* of 0.042–0.059 mol m⁻³^[17,22,39] ($T = 295\text{--}298\text{ K}$). The surfactant concentration was above *cmc* in all emulsions. It can be assumed that all emulsions have a saturated droplets interface, with an excess of surfactant to form micelles. The emulsions were stable over several weeks and showed no aging effects, such as coalescence, Ostwald ripening, or emulsion breakup. $T_{m,hex} = 291\text{ K}$ was used as melting temperature of n-hexadecane^[40], while different values of $T_{m,hex}$ can be found in literature (see, e.g., Himran et al.^[41]). The differential scanning calorimetry (DSC) measurements revealed that $T_{m,hex}$ was not significantly influenced due to the appearance as droplets.

A gear dispersing machine (T25 digital, IKA[®]-Werke GmbH & Co. KG, Staufen, Germany) was used for emulsion production. All emulsions were dispersed at 13.3 m s⁻¹ tangential speed (20,000 rpm, 12.7 mm outer diameter of the rotating part) for 5 min at room temperature for creating a reproducible droplet size distribution. The DSD of each emulsion was determined using a Mastersizer 3000E (Malvern Panalytical Ltd, Worcester, United Kingdom) (Figure S3).

The binary solutions consisted of TW20 and D₂O. They were homogenized using a magnetic stirrer at 800 rpm for 30 s just before the sample was taken.

5.2 | NMR measurements

A 400 MHz spectrometer (Ultrashield, Avance Neo, Bruker BioSpin, Germany) equipped with a DiffBB probe was used for NMR measurements. A liquid N₂ tank was connected to the probe via a transfer line, and the

regulation of the liquid N₂ flow was controlled by the Bruker Variable Temperature Unit (BVT, Bruker BioSpin, Germany) to temper the sample. The evaporation rate was constantly set to 2%.

A sample of 200 μl was measured to reduce temperature gradients within the sample and, as a result, reducing convection. The sample was placed centrally within the homogeneous area of the magnetic field and the radio-frequency coil.

A calibration according to Ammann et al.^[42] was performed to determine the sample temperature. Ethylene glycol (ROTIPURAN[®], Carl Roth, Karlsruhe, Germany, purity ≥ 99.5%) was used to measure the temperature within the sample tube via the difference in the chemical shift between the -OH and the -CH₂ ¹H peak maxima.

The solid fraction of n-hexadecane was determined by ¹H spectroscopy comparable to^[9] (Table 2). Only the liquid part of the dispersed phase was measurable within these experiments due to the short T_2 relaxation times of solids. The residual water was used as a reference as the concentration of water was constant during the experiment. The solid fraction of n-hexadecane droplets ξ_{hex} at a time t was calculated as

$$\xi_{hex}(t) = 1 - \frac{A_{hex}(t) \cdot A_{water}(t=0)}{A_{hex}(t=0) \cdot A_{water}(t)}, \quad (7)$$

where A_{hex} is the integral of the CH₂ and CH₃ peaks and A_{water} the integral of the H₂O peak (cf. Figure 15) calculated by a trapezoidal method implemented in MATLAB (R2021b, the MathWorks Inc., Natick, Massachusetts, United States). The upper and lower boundaries for each component are listed in Table 1.

All emulsion measurements were done at a constant temperature of $T = 289\text{ K}$, which is below the melting temperature of n-hexadecane ($T_{m,hex} = 291\text{ K}$, own DSC measurements, following Zhang et al.^[40]). The emulsions were thermocycled between 289 K (no spontaneous crystallization) and $T_c = 278.6\text{ K} \pm 1\text{ K}$ (spontaneous crystallization) to increase the solid fraction of the dispersed phase stepwise (Figure 16). The binary mixtures were also handled the same way for reproducibility.

To guarantee and prove that no further freezing or thawing of droplets takes place during the measurements, the samples were measured in the following order: spectroscopy – diffusometry – spectroscopy – T_2 -relaxometry – spectroscopy.

The PFG-STE sequence^[43] was used to measure diffusion (Figure 17b; Table 2). The transverse relaxation rate was measured by the CPMG pulse sequence^[27] (Figure 17c; Table 3), while spectra were recorded by the FID of a single pulse sequence (Figure 17a; Table 2).

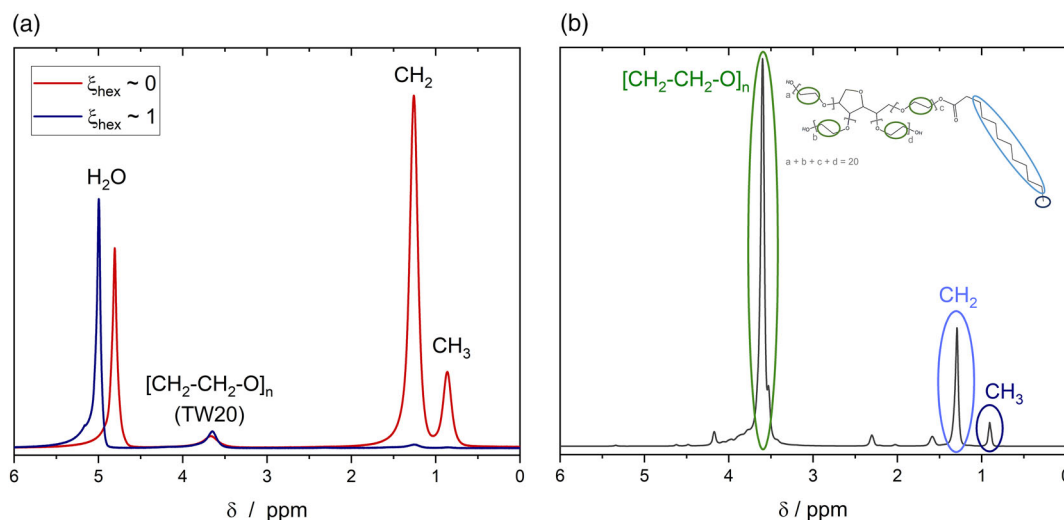


FIGURE 15 (a) ^1H spectra of an n-hexadecane-in-water emulsion, stabilized with TW20. The ^1H of the $[\text{CH}_2\text{-CH}_2\text{-O}]_n$ groups reflect the behavior of the surfactants' head groups in relaxation and diffusion measurements, while the CH_2 and CH_3 peaks mostly reflect $\xi_{\text{hex}}(t)$ and the residual water peaks indicate the measurement temperature. For better readability, the peak at 3.65 ppm is called the “TW20 peak.” (b) ^1H spectrum of pure TW20 with the corresponding chemical structure of TW20. Three peaks are highlighted in the spectrum and the chemical structure: CH_2 , CH_3 (both mainly representing n-hexadecane), and the CH_2 of the surfactants' polyether chains.

TABLE 1 Integration limits for data analysis of the spectra. All measurements were referenced to the signal of the CH_2 group at 1.26 ppm

Substance	Lower limit/ppm	Upper limit/ppm
Water (H_2O)	4.4	6.0
N-hexadecane ($\text{C}_{16}\text{H}_{34}$)	0.0	3.0
Head group of Tween [®] 20 ($\text{C}_{58}\text{H}_{114}\text{O}_{26}$) – polyether chain	3.0	4.4

5.3 | Data modeling

The measured signal decays of both relaxation and diffusion measurements were modeled using Origin 2021 (OriginLab Corporation, Northampton, United States). The various gamma distributions were implemented into Origin and the Levenberg–Marquardt iteration algorithm was used. The coefficient of determination R^2 was larger than 96% for all results presented in this paper.

5.4 | SAXS measurements

The SAXS (Xeuss 2.0, Xenocs SAS, Grenoble, France) measurements were done to reveal the structure of the micelles. Two samples were analyzed: one binary system containing only D_2O and TW20 (2 wt%) as a reference and one sample where only the continuous phase of a previously ternary emulsion system was present. The

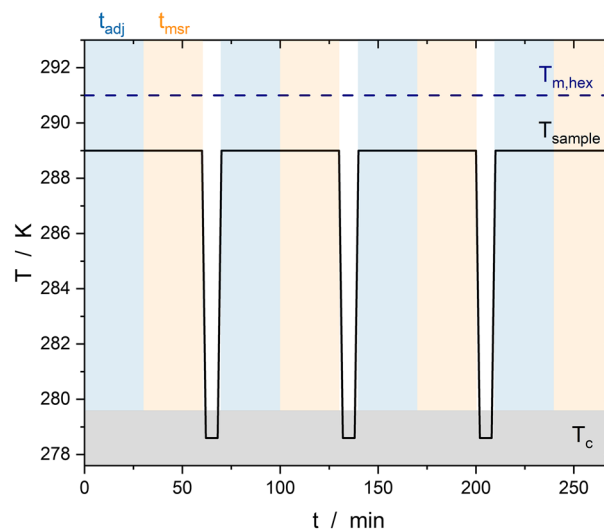


FIGURE 16 Schematic temperature profile for thermocycling of the samples. To increase the solid fraction, the sample (T_{sample}) was cooled down to T_c (grey region). All measurements were done below the melting point of n-hexadecane ($T_{m,\text{hex}}$) to exclude thawing of particles. The sample was tempered for 30 min (t_{adj} , blue region) and then measured (t_{msr} , orange region).

sample was centrifuged (2-16KCH, Sigma Laborzentrifugen GmbH, Osterode am Harz, Germany) at 8,000 rpm for 10 min at 20°C to separate the continuous and dispersed phases from each other. The continuous phase at the bottom of the flask was separated and rested for another 72 h. The sample was filtrated before analysis using a filter with a pore size of 200 nm to exclude any

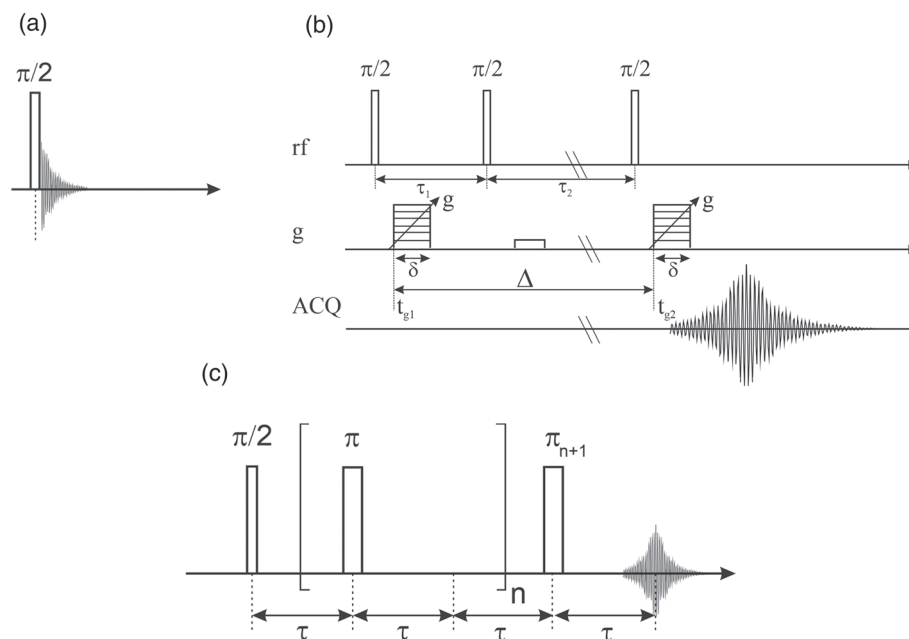


FIGURE 17 Schemes of the pulse sequences for (a) single pulse sequence for ^1H spectroscopy, (b) PFG-STE, and (c) CPMG

TABLE 2 Important pulse sequence parameters for ^1H NMR spectra and PFG-STE measurements as they were used for the different substance classes

Substance system	Emulsions/binary mixtures	Emulsions/suspensions	Binary mixtures
Pulse sequence	^1H -single pulse	PFG-STE	PFG-STE
Number of averages [–]	16	8	32–64
Repetition time [s]	4	4	4
Data points [–]	16 k	8 k	8 k
Diffusion time Δ [ms]		100	100
Number of gradient increments [–]		16	32
Effective gradient duration δ [ms]		2	2
Gradient amplitude g [T m^{-1}]		[0.15, ..., 3.00]	[0.019, ..., 0.6]
Measurement time [min]	1 min 30 s	8 min 32 s	34 min 8 s – 1 h 42 min 24 s

n-hexadecane droplets while guaranteeing the presence of micelles.

The SAXS device was equipped with a vacuum-tight sample holder (optical path length 1.5 mm). The distance between the sample and detector amounted to 1,750 mm. A Pilatus 300 K-S detector collected the data for 1,800 s. The signal intensity $I(q_{\text{SAXS}})$ was measured as a function of the scattering vector q_{SAXS} :

$$q_{\text{SAXS}} = \frac{4\pi}{\lambda} \sin\left(\frac{\theta}{2}\right). \quad (8)$$

θ represents the scattering angle and λ the wavelength of the Cu-K α X-ray beam ($\lambda = 0.154$ nm). The intensity detected also depends on the micellar volume N_{mic} and

TABLE 3 Important pulse sequence parameters for CPMG measurements as they were used for emulsions/suspensions and binary mixtures

Substance system	Emulsions/suspensions	Binary mixtures
Pulse sequence	CPMG	CPMG
Number of averages [–]	8	16
Repetition time [s]	4	4
FID-data points [–]	4 k	8 k
Number of increments [–]	32	32
Measurement time [min]	18 min 37 s	25 min 3 s
Half echo time [ms]	2	2
Last echo number [–]	156	122

the inverse micellar number concentration $(NV^{-1})_{mic}$. The intensity $I(q)$ is given by

$$I(q) \sim (NV^{-1})_{mic} \cdot N_{mic} \cdot \Delta\rho_e, \quad (9)$$

with the electron density difference $\Delta\rho_e$. A size distribution model was approximated to the data using the Software IgorPro 8 and the package Irena to extract the micellar size distribution. The Bragg equation (Equation 10) was used to estimate the layer thickness of the micelles:

$$l_{mic} = \frac{\lambda}{2 \cdot \sin\left(\frac{2\theta}{2}\right)}. \quad (10)$$

The form factor P_{mic} of the micelles was determined above the Guinier regime and found to differ between the reference ($P_{mic,ref} \sim 1.1$) and the sample ($P_{mic,sample} \sim 2.4$). The fit function was

$$I(q_{SAXS}) = m \cdot q_{SAXS}^{-P}, \quad (11)$$

with m representing the slope of $I(q_{SAXS})$ ^[44].

5.5 | DSC measurements

The DSC measurements (DSC Q2000, TA Instruments, New Castle, DE, United States) with a heating/cooling rate of 5 K min⁻¹ were used to determine the melting point of the surfactant to ensure that only the crystallization of the dispersed phase takes place.

5.6 | Viscosity measurements

The dynamic viscosity of the binary TW20-D₂O system was measured using a Physica MCR 301 rheometer (Anton Paar, Graz, Austria). It was equipped with a double-slit geometry (DG 26.7) with a slit width of 2 mm. The cylinder height was 40 mm.

ACKNOWLEDGEMENTS

The Deutsche Forschungsgemeinschaft is thanked for the substantial financial contribution in form of NMR instrumentation and within the instrumental facility Pro²NMR. We also would like to thank Sabrina Herberger (Institute for Thermal Process Engineering, Karlsruhe Institute of Technology, Germany) for doing the DSC measurements. Open Access funding enabled and organized by Projekt DEAL.

CONFLICT OF INTEREST

The authors have declared no conflict of interest.

ORCID

Gina Kaysan  <https://orcid.org/0000-0002-6773-7803>

Gisela Guthausen  <https://orcid.org/0000-0002-6444-2663>

Matthias Kind  <https://orcid.org/0000-0002-7203-1776>

REFERENCES

- [1] a) R. H. Müller, R. Shegokar, C. M. Keck, *Curr. Drug Discov. Technol.* **2011**, 8, 207; b) R. H. Müller, R. D. Petersen, A. Hommoss, J. Pardeike, *Adv. Drug Deliv. Rev.* **2007**, 59, 522; c) J. Pardeike, A. Hommoss, R. H. Müller, *Int. J. Pharm.* **2009**, 366, 170; d) D. J. McClements, *Adv. Colloid Interface Sci.* **2012**, 174, 1; e) J. Weiss, E. A. Decker, D. J. McClements, K. Kristbergsson, T. Helgason, T. Awad, *Food Biophys.* **2008**, 3, 146; f) R. Müller, *Eur. J. Pharm. Biopharm.* **2000**, 50, 161; g) P. E. Romero, J. Arribas-Barrios, O. Rodríguez-Alabanda, R. González-Merino, G. Guerrero-Vaca, *CIRP J. Manuf. Sci. Technol.* **2021**, 32, 396.
- [2] K. Köhler, H. P. Schuchmann (Eds), *Emulgiertechnik. Grundlagen, Verfahren und Anwendungen*, Behr, Hamburg **2012**.
- [3] J. N. Israelachvili, D. J. Mitchell, B. W. Ninham, *J. Chem. Soc., Faraday Trans. 2* **1976**, 72, 1525.
- [4] C. Tanford, *J. Phys. Chem.* **1972**, 76, 3020.
- [5] a) P. Saveyn, E. Cocquyt, W. Zhu, D. Sinnaeve, K. Haustraete, J. C. Martins, P. van der Meeren, *Phys. Chem. Chem. Phys.* **2009**, 11, 5462; b) J. D. McClements, E. Dickinson, M. Povey, *Chem. Phys. Lett.* **1990**, 172, 449; c) D. Langevin, *Emulsions, Microemulsions and foams*, Springer International Publishing, Berlin **2020**.
- [6] L. Guardia, J. I. Paredes, R. Rozada, S. Villar-Rodil, A. Martínez-Alonso, J. M. D. Tascón, *RSC Adv.* **2014**, 4, 14115.
- [7] a) G. Kaysan, N. Schork, S. Herberger, G. Guthausen, M. Kind, *Magn. Reson. Chem.* **2021**, 7, 615; b) D. J. McClements, S. R. Dungan, *J. Colloid Interface Sci.* **1997**, 186, 17.
- [8] G. Kaysan, A. Rica, G. Guthausen, M. Kind, *Crystals* **2021**, 11, 1471.
- [9] G. Kaysan, B. Spiegel, G. Guthausen, M. Kind, *Chem. Eng. Technol.* **2020**, 43, 1699.
- [10] a) H. Bunjes, M. H. J. Koch, K. Westesen, *J. Pharm. Sci.* **2003**, 92, 1509; b) D. Kalnin, O. Schafer, H. Amenitsch, M. Ollivon, *Cryst. Growth Des.* **2004**, 4, 1283; c) J. M. Maruyama, F. A. S. D. M. Soares, N. R. D'Agostinho, M. I. A. Gonçalves, L. A. Gioielli, R. C. Da Silva, *J. Agric. Food Chem.* **2014**, 62, 2253; d) M. S. Miskandar, Y. C. Man, R. A. Rahman, I. N. Aini, M. Yusoff, *J. Food Lipids* **2007**, 14, 1; e) D. Kashchiev, D. Clause, C. Jolivet-Dalmazzone, *J. Colloid Interface Sci.* **1994**, 165, 148.
- [11] a) M. Röding, D. Bernin, J. Jonasson, A. Särkkä, D. Topgaard, M. Rudemo, M. Nydén, *J. Magn. Reson.* **2012**, 222, 105; b) M. Röding, N. H. Williamson, M. Nydén, *J. Magn. Reson.* **2015**, 261, 6; c) N. H. Williamson, M. Nydén, M. Röding, *J. Magn. Reson.* **2016**, 267, 54.
- [12] a) O. Annunziata, L. Costantino, G. D'Errico, L. Paduano, V. Vitagliano, *J. Colloid Interface Sci.* **1999**, 216, 16; b) V. P.

- Arkipov, R. V. Arkipov, N. A. Kuzina, A. Filippov, *Magn. Reson. Chem.* **2021**, 59, 1126.
- [13] E. Förster, H. Nirschl, G. Guthausen, *Appl. Magn. Reson.* **2017**, 48, 51.
- [14] a) N. J. Turro, A. Yekta, *J. Am. Chem. Soc.* **1978**, 100, 5951; b) S. Freire, J. Bordello, D. Granadero, W. Al-Soufi, M. Novo, *Photochem. Photobiol. Sci.* **2010**, 9, 687.
- [15] E. S. Basheva, P. A. Kralchevsky, K. D. Danov, K. P. Ananthapadmanabhan, A. Lips, *Phys. Chem. Chem. Phys.* **2007**, 9, 5183.
- [16] E. O. Stejskal, J. E. Tanner, *J. Chem. Phys.* **1965**, 42, 288.
- [17] D. Linke, *Methods in enzymology*, Elsevier, Amsterdam, Netherlands **2009**, 603.
- [18] W. Al-Soufi, L. Piñeiro, M. Novo, *J. Colloid Interface Sci.* **2012**, 370, 102.
- [19] E. Sutherland, S. M. Mercer, M. Everist, D. G. Leaist, *J. Chem. Eng. Data* **2009**, 54, 272.
- [20] F. Luschtinetz, C. Dosche, *J. Colloid Interface Sci.* **2009**, 338, 312.
- [21] A. B. Mandal, S. Gupta, S. P. Moulik, *Indian J. Chem.* **1985**, 24A, 670.
- [22] C. Carnero Ruiz, J. Molina-Bolivar, J. Aguiar, G. MacIsaac, S. Moroze, R. Palepu, *Colloid Polym. Sci.* **2003**, 281, 531.
- [23] E. Hildebrandt, J.-H. Sommerling, G. Guthausen, K. Zick, J. Stürmer, H. Nirschl, G. Leneweit, *Colloids Surf. A Physicochem. Eng. Asp.* **2016**, 505, 56.
- [24] a) A. Einstein, *Ann. Phys.* **1905**, 8, 549; b) G. G. Stokes, *Trans. Camb. Philos. Soc.* **1850**, 9, 8.
- [25] A. Pal, N. Deenadayalu, S. Chaudhary, *Fluid Ph. Equilibria* **2015**, 391, 67.
- [26] B. Lindman, H. Wennerström, *Topics in current chemistry*, Springer-Verlag, Berlin/Heidelberg **1980**, 1.
- [27] S. Meiboom, D. Gill, *Rev. Sci. Instrum.* **1958**, 29, 688.
- [28] J. Plaß, Dissertation, Rheinisch-Westfälische Technische Hochschule Aachen, Aachen, **2001**.
- [29] X. Guan, K. Hailu, G. Guthausen, F. Wolf, R. Bernewitz, H. P. Schuchmann, *Eur. J. Lipid Sci. Technol.* **2010**, 112, 828.
- [30] R. Bernewitz, X. Guan, G. Guthausen, F. Wolf, H. P. Schuchmann, *Magnetic resonance in food science*, Royal Society of Chemistry, Cambridge **2011** 39.
- [31] a) A. Abragam, *The principles of nuclear magnetism*, University Press, Oxford **1983**; b) R. Kimmich, *NMR. Tomography, Diffusometry, Relaxometry*, Springer, Berlin, Heidelberg **1997**; c) M. Mehring, *Principles of high resolution NMR in solids*, Springer, Berlin, Heidelberg **1983**.
- [32] J. Penfold, R. K. Thomas, P. X. Li, J. T. Petkov, I. Tucker, J. R. P. Webster, A. E. Terry, *Langmuir* **2015**, 31, 3003.
- [33] J. Brinck, B. Jönsson, F. Tiberg, *Langmuir* **1998**, 14, 1058.
- [34] A. Bąk, W. Podgórska, *Colloids Surf. A Physicochem. Eng. Asp.* **2016**, 504, 414.
- [35] J. Weiss, J. N. Coupland, D. J. McClements, *J. Phys. Chem.* **1996**, 100, 1066.
- [36] S. R. Dungan, B. H. Tai, N. I. Gerhardt, *Colloids Surf. A Physicochem. Eng. Asp.* **2003**, 216, 149.
- [37] T. El Rhafiki, T. Kousksou, A. Jamil, S. Jegadheeswaran, S. D. Pohekar, Y. Zeraouli, *Sol. Energy Mater. Sol. Cells* **2011**, 95, 2588.
- [38] N. R. Biswal, J. K. Singh, *RSC Adv.* **2016**, 6, 113307.
- [39] A. Patist, S. S. Bhagwat, K. W. Penfield, P. Aikens, D. O. Shah, *J. Surfactant Deterg.* **2000**, 3, 53.
- [40] P. Zhang, Z. W. Ma, R. Z. Wang, *Renew. Sustain. Energy Rev.* **2010**, 14, 598.
- [41] a) S. Himran, A. Suwono, G. A. Mansoori, *Energy Source.* **1994**, 16, 117; b) R. L. Snow, J. B. Ott, J. R. Goates, K. N. Marsh, S. O'Shea, R. H. Stokes, *J. Chem. Thermodyn.* **1986**, 18, 107.
- [42] C. Ammann, P. Meier, A. E. Merbach, *J. Magn. Reson.* **1982**, 319, 46.
- [43] J. E. Tanner, *J. Chem. Phys.* **1970**, 52, 2523.
- [44] a) M. Meier, J. Ungerer, M. Klinge, H. Nirschl, *Powder Technol.* **2018**, 339, 801; b) G. Beaucage, *J. Appl. Cryst.* **1995**, 28, 717; c) G. Beaucage, D. W. Schaefer, *J. Non Cryst. Solids* **1994**, 172-174, 797.

SUPPORTING INFORMATION

Additional supporting information can be found online in the Supporting Information section at the end of this article.

How to cite this article: G. Kaysan, R. Kräling, M. Meier, H. Nirschl, G. Guthausen, M. Kind, *Magn Reson Chem* **2022**, 1. <https://doi.org/10.1002/mrc.5305>